Temporal Embryonic Origin Critically Determines Cellular Physiology in the Dentate Gyrus

Laurène Save, Agnès Baude, Rosa Cossart

Cerebral Cortex, 2018; 1–14

doi: 10.1093/cercor/bhy132
Original Article

ORIGINAL ARTICLE

Temporal Embryonic Origin Critically Determines Cellular Physiology in the Dentate Gyrus

Laurène Save[1,2,3], Agnès Baude[1,2,3] and Rosa Cossart[1,2,3]

[1]Inserm, Marseille 13009, France, [2]Aix-Marseille University, UMR 1249, Marseille 13009, France and [3]INMED, Marseille 13009, France

Address correspondence to Rosa Cossart, INMED–INSERM UMR1249, 163 Avenue de Luminy, BP 13, 13273 Marseille cedex 9, France.
Email: rosa.cossart@inserm.fr

Agnès Baude and Rosa Cossart share senior authorship

Abstract

The dentate gyrus, the entry gate to the hippocampus, comprises 3 types of glutamatergic cells, the granule, the mossy and the semilunar granule cells. Whereas accumulating evidence indicates that specification of subclasses of neocortical neurons starts at the time of their final mitotic divisions, when cellular diversity is specified in the Dentate Gyrus remains largely unknown. Here we show that semilunar cells, like mossy cells, originate from the earliest stages of developmental neurogenesis and that early born neurons form age-matched circuits with each other. Besides morphology, adult semilunar cells display characteristic electrophysiological features that differ from most neurons but are shared among early born granule cells. Therefore, an early birthdate specifies adult granule cell physiology and connectivity whereas additional factors may combine to produce morphological identity.

Key words: dentate gyrus, development, electrophysiology, mossy cell, semilunar cell

Specification of cardinal neuronal subclasses is a well-studied process in the neocortex. There, increasing evidence from the last 4 decades indicates that neuronal identity is predetermined as early as final mitotic divisions occurring in the embryonic proliferative regions, with the underlying genomic mechanisms being partly elucidated (Butt et al. 2005; Rakic et al. 2009; Nord et al. 2015). Whether the concept of the protomap (Rakic 1972, 1988) applies to other cortical regions such as the hippocampus remains an open question. Dentate granule cells are the principal components of the dentate gyrus (DG), which is the critical entry point to the hippocampus. Much attention has been given to adult neurogenesis in this region because it is 1 of only 2 brain areas where it occurs in nonhuman mammals and in particular in rodents (Donega et al. 2018). The continuous addition of new granule cells in rodents makes the DG a highly heterogeneous structure composed of different generations of neurons. If developmental and adult-born neurons were shown to be similar regarding their intrinsic and synaptic properties (Laplagne et al. 2006, 2007), the age of adult-born neurons is known to critically determine their function and excitability. Hence, for example, young adult-born granule cells are more excitable (Schmidt-Hieber et al. 2004), support pattern separation (Nakashiba et al. 2012), but are less spatially tuned (Danielson et al. 2016) and more prone to reactive plasticity during epileptogenesis (Kron et al. 2010) compared with older ones.

Whether such age-dependent specialization of function also applies to developmental neurogenesis remains unknown. This is a particularly important issue since most granule cells originate from developmental neurogenesis (Altman and Bayer 1990; Mathews et al. 2010) with a peak at P1 in mice and P7 in rats, and since neurons originating from the earliest stages of developmental neurogenesis were recently shown to be more prone to coordinate neuronal activity in the CA3 hippocampal region (Picardo et al. 2011; Marissal et al. 2012). Interestingly, it is known that granule cells are a heterogeneous cell population,

both morphologically and functionally. Of particular interest are the semilunar granule cells (SGC), a name coined by Ramon y Cajal (1909) alluding to their characteristic cell body shape and dendritic arborization. These cells are a rare subtype of granule cells with a soma in the inner molecular layer, and a dendritic arbor shaped like a half-moon. Remarkably, these cells were shown to be important vectors for the transfer of entorhinal inputs to the hippocampus through specific intrinsic properties and a differential connectivity pattern, including a distinctive integration into local GABAergic circuits (Williams et al. 2007; Larimer and Strowbridge 2010; Gupta et al. 2012).

Given their prominent network function and their characteristic morphology, we therefore asked whether this subtype of granule cells could be specified through their developmental ontogenetic origin. Using inducible genetic fate mapping to label glutamatergic neurons in the DG according to their birthdate, we show that SGC, like mossy cells (MC) (Li et al. 2008), originate from the earliest stages of DG developmental neurogenesis, with an ontogenesis peak about 1 week before that of granule cell developmental ontogenesis. Accordingly, these cells gain mature properties at early postnatal stages. In addition, multidimensional clustering of physiological variables sampled from early born and randomly targeted granule cells (GC) in the adult, segregated pioneer GC into a physiologically distinct group that includes semilunar cells. This subclass of early born GC (ebGC) is anatomically heterogeneous but shares similar intrinsic properties all converging towards a lower excitability compared with most granule cells. In addition, ebGC are evenly distributed around the granular layer and display putative axonal contacts onto hilar MC. Therefore, a subclass of pioneer developmental granule cells that includes ebGC synapsing onto MC, is physiologically, but not anatomically, specified by an early developmental origin. Although the specific contribution of this pioneer circuit to DG function remains to be determined, this study further extends the developmental scheme by which early born neurons are likely to become key components of adult hippocampal networks. It also partially extends the "protomap hypothesis" to the early generated cohort of DG cells by showing that physiological diversity is probably predetermined at the time of origin whereas other factors contribute to the specification of morphological traits.

Materials and Methods

Inducible Genetic Fate Mapping

All protocols were performed under the guidelines of the French National Ethics Committee for Sciences and Health report on "Ethical Principles for Animal Experimentation" in agreement with the European Community Directive 86/609/EEC under agreement #01 413.03. All efforts were made to minimize pain and suffering and to reduce the number of animals used. In order to birthdate developmentally generated glutamatergic cells in the DG, we used the fact that most cortical glutamatergic neurons originate from progenitors expressing a combination of transcription factors including the proneural bHLH transcription factor Neurogenin2 (*Ngn2*). *Ngn2* is expressed in both neuronal progenitors and early postmitotic neurons in the VZ and SVZ (Hand et al. 2005). *Ngn2* expression is transitory and rapidly downregulated as soon as cells leave the cell cycle and start migrating towards their ultimate position (Hand et al. 2005; Ozen et al. 2007; Galichet et al. 2008). To follow the fate of glutamatergic neurons within the adult DG, *Ngn2Cre*$^{ERTM/wt}$/*Ai14:LoxP*$^{+/+}$ (Zirlinger et al. 2002; Miyoshi et al. 2010) male mice were crossed with 7–8-week-old wild-type Swiss females (C.E Janvier, France) for offspring production. To induce Cre activity during embryogenesis, tamoxifen was delivered to pregnant mothers (2 mg per 30 g of body weight of tamoxifen solution,10 mg/mL prepared in corn oil Sigma, St. Louis, MO) at embryonic days E10.5, 12.5, 14.5, 16.5 postvaginal plug. To induce postnatal Cre activity, P0 (postnatal day-0), P1, P3, and P7 pups were intraperitoneally injected with the tamoxifen solution. Recombination of the reporter allele is achieved within 24 h upon administration of tamoxifen. For simplification purposes *Ngn2*$^{CreERTM/wt}$/*Ai14:LoxP*$^{+/wt}$ mice pups expressing Td-tomato are named tamoxifen-treated *Ngn2/Ai14*. We assessed unspecific labeling in pups issued from nontamoxifen-gavaged mothers. We show that the "leaky" expression resulting in nontamoxifen-dependent Cre-mediated recombination (Madisen et al. 2010) is negligible (0.8% of Td-Tomato expressing cells, $n = 10$ brains).

Table 1 Electrophysiological properties of ebGC or GC in young adult

	ebGC	GC	*P* values
Number of cells	40	67	
Rm (MΩ)	217 ± 18.24	272 ± 15.25	0.0018
Cm (pF)	71.02 ± 4.61	72.22 ± 5.05	0.5598
AP threshold (mV)	−32.94 ± 1.16	−35.61 ± 0.91	0.0362
AP amplitude (mV)	76.26 ± 1.52	81.22 ± 1.39	0.0023
AP duration (ms)	1.08 ± 1.19	1.39 ± 0.08	0.0828
Vrest (mV)	−70.37 ± 1.24	−70.83 ± 1.16	0.5036
fAHP (mV)	16.97 ± 0.77	16.24 ± 0.75	0.9411
Accommodation (mV)	16.35 ± 1.43	14.93 ± 0.98	0.4611
Gain (Hz/pA)	3.28 ± 0.48	6.39 ± 0.77	0.0279
Max. firing rate (Hz)	6.06 ± 1.02	9.04 ± 0.79	0.0076
% of adaptation	38.65 ± 4.28	30.58 ± 3.73	0.1278
Rheobase (pA)	156.8 ± 13.7	102.7 ± 9	0.0005

P values as given by Mann and Whitney test. All data are given as mean ± SEM. AP, action potential; Cm, membrane capacitance; Rm, membrane resistance; Vrest, resting membrane potential; fAHP, fast after hyperpolarization.

Statistical Analysis

All the data reported in the tables (Tables 1–4) are given as mean ± standard error of the mean (SEM). All the data shown in scatter dot plots or histograms are given as mean ± standard deviation (SD) (Figs 2–5). All statistical analyses were performed with the GraphPad Prism 7 software using non parametric Mann and Whitney tests, or Kruskall Wallis tests followed by Dunn's multiple comparisons test. *P* values are given in Tables 1–4, or indicated on graphs as * for $P < 0.05$; ** for $P < 0.01$; *** for $P < 0.005$; **** for $P < 0.001$.

Morphological Analysis

Mice aged between postnatal days 34 and 100 (P34–100; mean P62 ± 3, $n = 37$) tamoxifen-treated *Ngn2/Ai14* animals were deeply anesthetized with a ketamine (250 mg/kg) and xylazine (25 mg/kg) solution (i.p.) and transcardially perfused (1 mL/g) with 4% paraformaldehyde in saline phosphate buffer (PBS). Brains were post-fixed overnight, then washed in PBS.

Quantification and Distribution of Fate Mapped Granule Cells

The 70 µm-thick horizontal or coronal sections of fixed brains were sliced (total 34 mice, P34–P100, mean P63± 2; E10.5, $n = 2$

Table 2 Morphological properties of SGC or GC in young adult

	SGC E12.5	GC E12.5	GC random	*P* values
Soma and dendrites				
# cells	17	10	26	
Soma perimeter (μm)	137.6 ± 8.3	112.0 ± 3.9	145.9 ± 5.1	0.001
# dendritic nodes	11.1 ± 0.8	12.4 ± 1.3	12.9 ± 0.5	0.1135
# dendritic ends	14.5 ± 0.8	13.5 ± 1.3	14.0 ± 0.6	0.3449
# Primary dendrites	3.6 ± 0.4	1.1 ± 0.1	1.1 ± 0.1	<0.0001
Dendritic length (mm)	5.6 ± 0.4	5.2 ± 0.3	7.38 ± 0.4	0.002
Angle spreading (°)	168.8 ± 8.4	108.0 ± 5.6	107.2 ± 5.7	<0.0001
Axon				
# recovered axons	5	4	11	
# nodes	5.2 ± 1.6	6.5 ± 1.3	5.8 ± 1.1	0.2443
# ends	6.2 ± 1.6	7.5 ± 1.3	6.8 ± 1.1	0.2443
Length (mm)	5.7 ± 1.3	3.3 ± 0.7	2.9 ± 0.4	0.4146

P values as given by Kruskal and Wallis test. All data are given as mean ± SEM.

Table 3 Electrophysiological properties of the 3 groups of SGC and GC as established after cluster analysis

	Cluster 1	Cluster 2	Cluster 3	*P* values
Number of cells	21	45	41	
Rm (MΩ)	442.1 ± 29	162.4 ± 4.7	248.0 ± 5.7	<0.0001
Cm (pF)	47.5 ± 5.8	88.8 ± 6.3	66.7 ± 3.7	<0.0001
AP threshold (mV)	−38.2 ± 1.2	−32.3 ± 1.2	−36.2 ± 1	0.0035
AP amplitude (mV)	81 ± 2.3	77.2 ± 1.8	80.4 ± 1.6	0.2573
AP duration (ms)	1.5 ± 0.13	1.0 ± 0.05	1.4 ± 0.1	0.0017
Vrest (mV)	−71.2 ± 1.8	−69.5 ± 1.4	−71.5 ± 1.3	0.0914
fAHP (mV)	16.1 ± 1.4	17.4 ± 0.9	14.7 ± 0.7	0.1202
Accommodation (mV)	16.4 ± 1.7	14.7 ± 1.2	15.5 ± 1.3	0.8114
Gain (Hz/pA)	7.0 ± 1	2.8 ± 0.4	6.8 ± 1	0.0005
Max. firing rate (Hz)	10.8 ± 1.2	5.5 ± 1	8.9 ± 1	0.0003
% of adaptation	16.1 ± 2	51.9 ± 5.4	29.1 ± 4.1	0.0003

P values are given by Kruskal and Wallis test. All data are given as mean ± SEM. AP, action potential; Cm, membrane capacitance; Rm, membrane resistance; Vrest, resting potential; fAHP, fast after hyperpolarization.

brains; E12.5, $n = 5$ brains; E14.5, $n = 5$ brains; E16.5, $n = 4$ brains; P0, $n = 4$ brains; P1, $n = 5$ brains; P3, $n = 5$ brains; P7, $n = 4$ brains). In order to quantify Td-tomato labeled neurons, granule cells, SGC, and MC were manually counted according to previously established morphological criteria (Larimer and Strowbridge 2010) using Zeiss AxioImager Z2 microscope. A total of 105 303 cells were counted including 102 136 granule cells, 2521 SGC, and 646 MC. The distribution of Td-tomato-labeled neurons throughout the granule cell layer after tamoxifen administration at different time points was assessed manually by estimating the position of the labeled cells within the thickness of the granular layer normalized to 1. The position was analyzed for a total of 2547 cells (E12.5, 5 brains, 133 cells; E14.5, 2 brains, 254 cells; E16.5, 2 brains, 103 cells; P0, 3 brains, 572 cells; P1, 2 brains, 777 cells, P3, 616 cells, P7, 3 brains, 92 cells). Therefore, a cell scoring at 0.5 is located in the middle of the granular layer while a score from 0.5 to 1 or from 0 to 0.5 located the cell towards the outer or inner part of the granular layer, respectively.

Immunocytochemistry

The 70 μm-thick brain sections from E12.5 tamoxifen-treated *Ngn2/Ai14* periadolescent mice ($n = 3$ mice, P42) were randomly examined to search for contacts between mossy fibers and MC within the hilus. Immunolabelling for PSD95 was used as a proxy for putative synaptic contacts between early born granule cells and MC in the hilus. E12.5 tamoxifen-treated *Ngn2/Ai14* mice were deeply anesthetized, perfused and brains were processed as previously described (Villette et al. 2016) using a rabbit anti-PSD95 antibody (1/1000; ab18258, Abcam; RRID: AB_444 362). Images were obtained using a Zeiss LSM 800 confocal microscope (488 and 561 nm laser wavelength, sequential scanning, pixel size 0.068 μm, *z* step 0.46 μm).

Morphological Analysis of Neurobiotin Filled Cells

A total of 53 and 14 Neurobiotin-filled neurons were recovered for morphological analysis from young adult mice aged between P37 and P171 (mean age: P88 ± 5, $n = 41$) and juvenile mice aged P15, respectively. Slices were fixed overnight at 4 °C in Antigenfix (www.diapath.com), rinsed in PBS containing 0.3% Triton X-100 (PBST) and incubated overnight at room temperature in Al488-streptavidin (1/1000 in PBST; Jackson Immunoresearch, West Grove, PA). Stacks of optical sections (pixel size 0.24 μm, *z* step = 0.4 μm) were collected using a Leica TCS SP5-X confocal microscope (488 nm laser wavelength). Neuronal reconstruction and post hoc analysis were performed with a computer-assisted system (Neurolucida, MicroBrightfield). Morphological variables included dendritic and axonal lengths, somatic, dendritic and axonal surfaces, number of dendritic and axonal endings and nodes, and dendritic angle spread.

Table 4 Morpho-physiological properties of SGC or GC at P15

	SGC E12.5	GC random	*P* values
Electrophysiology			
# cells	21	15	
Rm (MΩ)	232.5 ± 29.7	529.3 ± 65.7	0.0008
Cm (pF)	70.3 ± 7.6	41.8 ± 6.9	0.0057
AP threshold (mV)	−35.1 ± 1.4	−35.8 ± 1.6	0.6272
AP amplitude (mV)	80.4 ± 3.7	67.8 ± 4.1	0.0064
AP duration (ms)	1.1 ± 0.03	1.2 ± 0.1	0.068
Vrest (mV)	−65.7 ± 2.0	−68.3 ± 2.9	0.3720
fAHP (mV)	14.7 ± 1.6	17.8 ± 0.9	0.1935
Accommodation (mV)	14.0 ± 2.5	15.8 ± 3.1	0.7026
Gain (Hz/pA)	6.3 ± 1.4	16.8 ± 5.6	0.0979
Max. firing rate (Hz)	8.8 ± 1.6	14.1 ± 4.6	0.5953
% of adaptation	29.5 ± 6.9	20.9 ± 8.9	0.0278
Morphology			
Soma and dendrites			
# cells	5	9	
Soma perimeter (μm)	158.9 ± 9.6	148.0 ± 5.2	0.4191
# dendritic nodes	11.2 ± 1.3	15.6 ± 1.7	0.1074
# dendritic ends	14.8 ± 1.2	16.6 ± 1.8	0.6299
# Primary dendrites	3.4 ± 0.3	1.0 ± 0.0	0.0005
Dendritic length (mm)	5.8 ± 1.4	5.39 ± 0.7	0.9760
Angle spreading (°)	170 ± 11.4	108.8 ± 13.4	0.0101
Axon			
# recovered axons	3	2	
# nodes	1.7 ± 0.9	6.5 ± 0.5	0.2000
# ends	2.7 ± 0.9	7.5 ± 0.5	0.2000
Length (mm)	2.0 ± 0.4	2.9 ± 0.1	0.2000

P values as given by Mann and Whitney test. All data are given as mean ± SEM. AP, action potential; Cm, membrane capacitance; Rm, membrane resistance; Vrest, resting potential; fAHP, fast after hyperpolarization.

Electrophysiology

Horizontal hippocampal slices (350 μm) were prepared from young adult mice aged between P37 and P171 (mean age: P88 ± 5, n = 41) and P15 mice, wild-type for control or E12.5 tamoxifen-treated *Ngn2/Ai14*, with a Leica VT1200 Vibratome using the Vibrocheck module in ice-cold oxygenated modified artificial cerebrospinal fluid (0.5 mM CaCl2 and 7 mM MgSO4; NaCl replaced by an equimolar concentration of choline). Slices were then transferred for rest (1 h) in oxygenated normal aCSF containing (in mM): 126 NaCl, 3.5 KCl, 1.2 NaH_2PO_4, 26 $NaHCO_3$, 1.3 $MgCl_2$, 2.0 $CaCl_2$, and 10 D-glucose, pH 7.4. A total of 143 out of 193 cells within the DG were recorded in hippocampal slices of mice aged P15 (GC, n = 15; SGC, n = 21) and >P50 (GC, n = 82; SGC, n = 25) for physiological characterization. A total of 50 cells were discarded because it was necessary to inject too much negative current (<−10 pA) to hold them for stable recordings. Overall, 67 neurons were successfully recovered for morphological analysis (see above). Neurons were held in current-clamp using a patch-clamp amplifier (HEKA, EPC10) in the whole-cell configuration. Intracellular solution composition was (in mM): 130 K-methylSO$_4$, 5 KCl, 5 NaCl, 10 HEPES, 2.5 Mg-ATP, 0.3 GTP, and 0.5% Neurobiotin. No correction for liquid junction potential was applied. The osmolarity was 265–275 mOsm, pH 7.3. Microelectrodes resistance was 7–10 MΩ. Uncompensated access resistance was monitored throughout the recordings. Values below 20 MΩ were considered acceptable and the results were discarded if it changed by more than 20%. Whole-cell measurements were filtered at 3 kHz using a patch-clamp amplifier. Recordings were digitized online (10 kHz) with an interface card to a personal computer and acquired using Axoscope 7.0 software. For experiments examining the firing rate, capacitance, and input resistance, cells were held close to −75 mV, which corresponded to the resting membrane potential, that is, the value obtained in the absence of current injection. The test pulse consisted of 4 s incremented current injections with steps of 10 pA. The rheobase was defined as the minimal depolarizing current pulse intensity generating at least one action potential. Spike threshold, amplitude and duration (temporal width at half maximum amplitude) were calculated at the rheobase. Input resistance (Rm) and membrane time constant (Tm) were determined on responses to incremented hyperpolarizing current pulses from −5 to −50 pA (duration: 500 ms). Time constant was determined by fitting the voltage response to a single exponential and membrane capacitance (Cm) was calculated as Cm = Tm/Rm. Firing behavior was analyzed: 1) at the first step following rheobase; 2) at the step eliciting the maximum number of spikes (typically corresponding to 80 pA current injection from the rheobase from which the maximum firing rate value was calculated). Spike frequency adaptation ratio (adaptation %) was calculated as the ratio of the number of spikes occurring within the first 400 ms of the step divided by the total number of spikes evoked in response to a 80 pA current injection from the rheobase for 4 s. The gain was defined as the slope of the linear portion of the curve plotting evoked spike frequency as a function of injected current. Accommodation was defined as the voltage difference between the amplitude of the first and last evoked spikes for the 80 pA current injection from the rheobase. Fast after hyperpolarization (fAHP) was calculated as the amplitude in voltage of the first component of the after-hyperpolarization measured, at rheobase, as the difference between spike threshold and the negative peak of the AHP.

Cluster Analysis of Electrophysiological Parameters

The term "cluster analysis" refers to a set of multivariate exploratory statistical methods that group objects (cases) of a dataset based on their degree of similarity. All cases are first plotted in a multidimensional space defined by all the measured variables; we included in this study 11 physiological variables: membrane resistance, membrane capacitance, AP threshold, AP duration, AP amplitude, resting membrane potential, fAHP, accommodation, gain, maximum firing rate, and % of adaptation. A certain measure of proximity is chosen (distance), and clusters are eventually formed by the cases that fulfill the criteria of the clustering method selected. The cluster analysis was performed with Euclidean distances by using Ward's method (Statistica Software) only with SGC and GC (n = 107 out of 137 cells for which all the 11 parameters could be calculated) recorded in animals (see above) where the physiological variables were measured (Table 3). According to Ward's method, cases are assigned to clusters so that the variance (sum of squared deviation from the mean) within each cluster is minimized. The analysis resulted in 3 well-defined clusters.

Results

Early Born Granule Cells Evenly Integrate the Granular Layer

DG glutamatergic cells were fate-mapped using the *Ngn2*$^{CreERTM/wt}$/*Ai14:LoxP*$^{+/wt}$ transgenic mouse line (see Materials and Methods). Hence, by using the *Ngn2*^{CreERTM} driver and *Ai14* reporter lines and by providing tamoxifen at separate embryonic time points

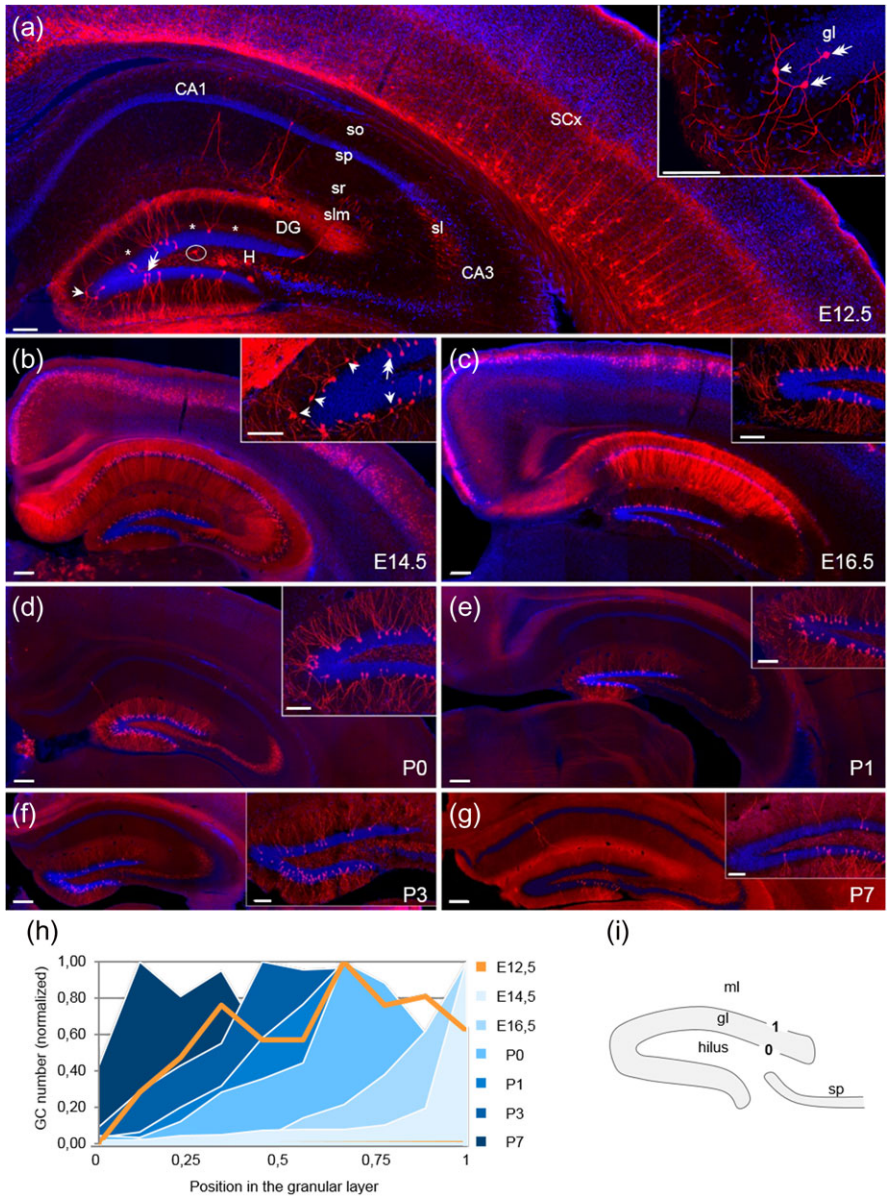

Figure 1. Fate mapping glutamatergic neurons in the dentate gyrus (DG). (*a–g*) Micrographs showing the distribution in the hippocampus and neocortex of fate-mapped neurons from young adult *Ngn2CreERTM;Ai14:LoxP* (Td-Tomato) mouse coronal brain slices following tamoxifen administration at various pre- (E12.5, E14.5, E16.5) and postnatal (P0–P7) time points. Within the DG, many SGC (inset, arrows) are visible after E12.5–E14.5 tamoxifen administration as well as numerous GC (double arrows). Note the presence of labeled fibers in the inner molecular layer (i.e., stars) after E12.5 tamoxifen administration. SGC could barely be seen at later time points of tamoxifen administration. Mossy cells can be found in the hilus (H, circled area in *a*). Insets are higher magnification displays of the DG. Counterstaining was performed with DAPI (blue). (*h*, *i*) Diagram showing the position of the soma of GC in the granular layer (gl) of the DG as a function of the date of tamoxifen administration. Cells located closer to the hilus are closer to the value 0, whereas cells that are closer to the molecular layer (ml) approach the value 1, as illustrated by the scheme (*i*). SCx, somatosensory cortex; sl, stratum lucidum; slm, stratum lacunosum moleculare; so, stratum oriens; sp, stratum pyramidale; sr; stratum radiatum. Scale bars = 200 μm, and 100 μm for insets.

(E10.5, $n = 2$ brains; E12.5, $n = 5$; E14.5, $n = 5$; E16.5, $n = 4$; P0, $n = 4$; P1, $n = 5$; P3, $n = 5$; P7, $n = 4$), we label temporally distinct populations of glutamatergic DG cells (Fig. 1*a–g*).

We first compared the somatic location of GC in the granular layer according to their fate-mapped date of birth (Fig. 1). For that, we calculated for each neuron ($n = 14$ brains, $n = 48$ hippocampal slices) the radial position of its soma relative to the hilus border divided by the full radial length of the granular layer. That number is therefore almost zero for cells close to the hilus while it is almost one for cells close to the inner molecular layer (Fig. 1*h*,*i*). We observed a progressive shift of that radial distribution from the inner molecular layer to the hilus as the age of the cells went from E14.5 to P7. In other words, from E14.5 to P7, successive generations of GC migrate past the existing earlier born neurons to occupy positions closer to the hilus thus creating layers in an "inside–out" fashion, in agreement with early work (Angevine 1965; Caviness 1973; Schlessinger et al. 1975; Bayer 1980; Rakic and Nowakowski 1981;

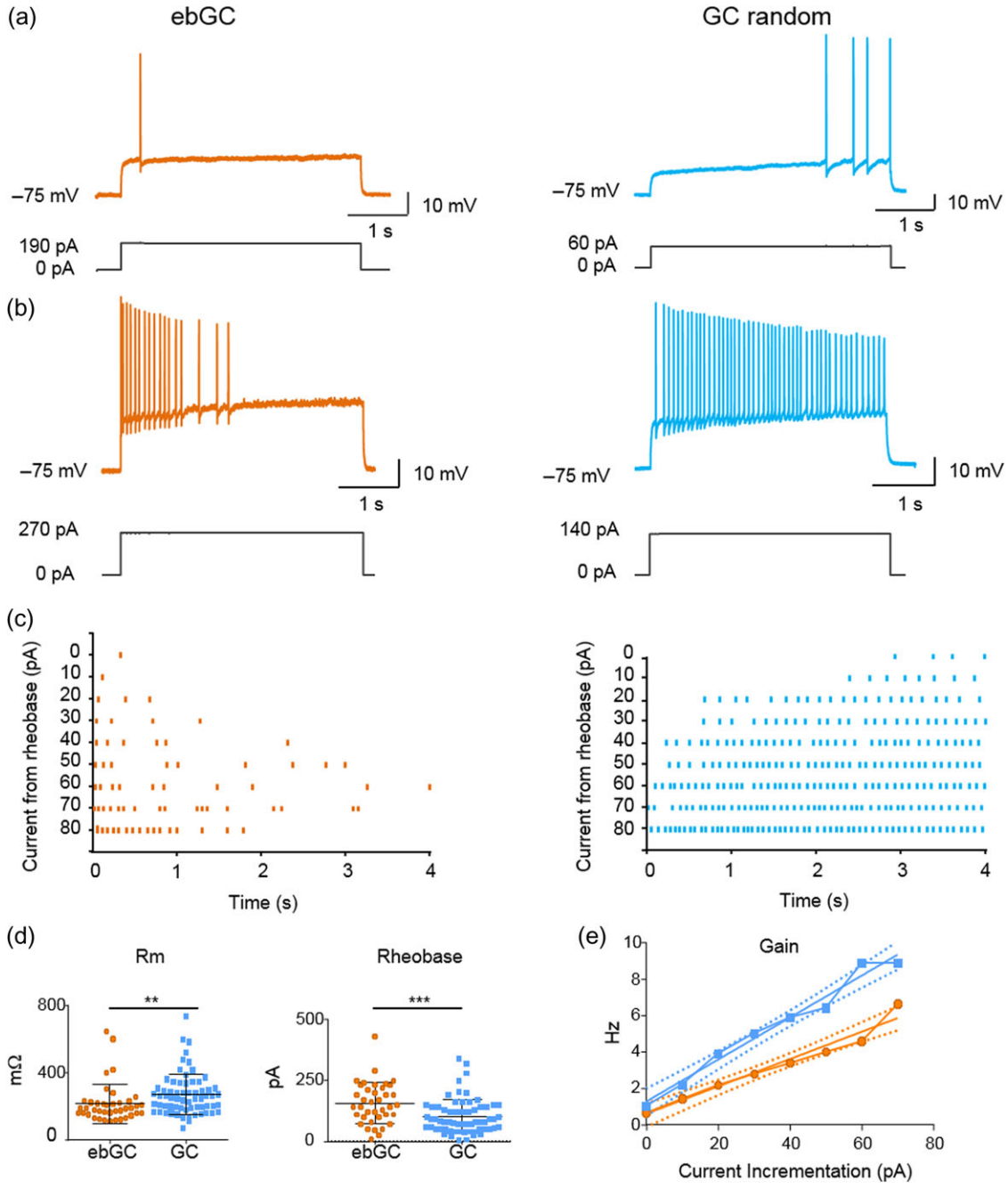

Figure 2. Early born granule cells (ebGC) display distinctive electrophysiological properties. (*a*) Representative examples of the evoked firing pattern at rheobase for an ebGC (orange) and a granule cell randomly recorded (GC, blue) in young adult hippocampal slices. Black traces indicate injected current. (*b*) Typical firing pattern at 80 pA from the rheobase. Black traces indicate injected current. (*c*) Rasterplots showing the timing of Action Potentials (small vertical lines) evoked by incremented positive current injections (4 s, 10 pA increment) from the rheobase (0 pA). (*d*) Scatter dot plots (mean ± SD) showing, from the left to the right, the membrane resistance (Rm) and the rheobase for ebGC and randomly recorded GC; ** and *** are *P* values < 0.01 and 0.001, respectively, as given by Mann and Whitney test. (*e*) Pooled *f/I* plots indicating the evoked firing rate as a function of current injected from the rheobase comparing ebGC (orange) and GC (blue). These are significantly different (*P* = 00007; dotted lines represent confidence bands).

Crespo et al. 1986; Mathews et al. 2010). Interestingly, this rule did not apply to earlier neurons labeled by E12.5 tamoxifen administration (GC E12.5) as they were found almost homogeneously distributed along the radial axis of the granule cell layer (Fig. 1*h*). These results therefore indicate that E12.5-labeled neurons stand apart in their positioning along the radial axis of the granule cell principal layer.

Early Born Granule Cells Display Distinct Electrophysiological Properties

We next asked whether the physiological characteristics of these early-born cells also differed from other GC. To this aim, early born developmental GC (ebGC) expressing Td-Tomato following tamoxifen supply at E12.5, were targeted for current-clamp recordings in hippocampal slices from young adult mice

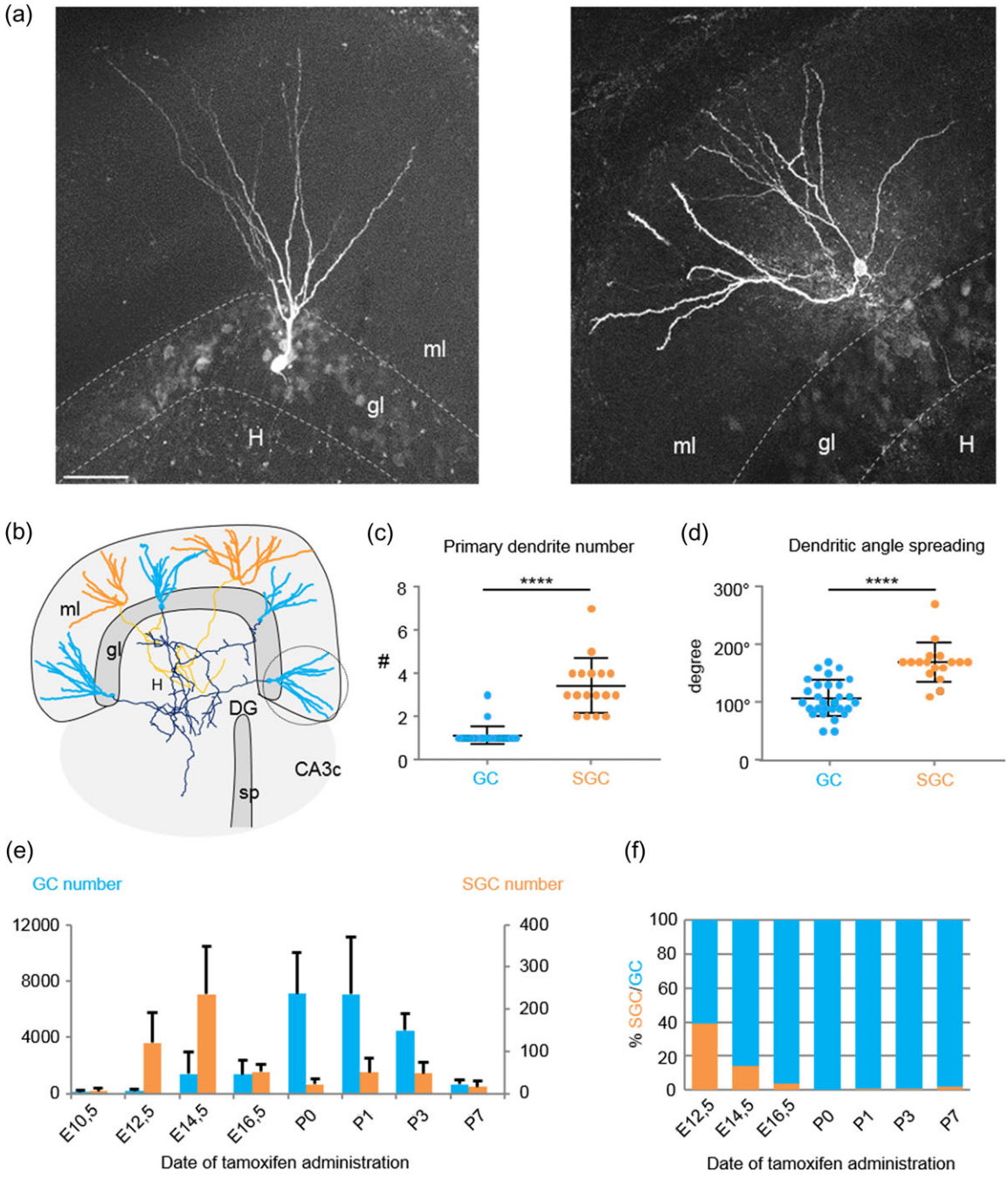

Figure 3. Early born granule cells segregate in 2 morphologically distinct cell subtypes. (*a*) Micrographs of 2 Neurobiotin-filled neurons, a GC in the granular layer (gl, left) and a SGC with a soma from which emerges the remarkable half-moon shaped dendritic arborization in the molecular layer (ml, right). Scale bar = 50 µm. (*b*) Neurolucida reconstructions of 3 randomly recorded GC (blue) and 3 early born cells with 2 SGC (orange, left, middle) and an ebGC (blue, dashed circle, right), placed on a schematic representation of the DG; the axons of reconstructed neurons (thinner lines) can be followed throughout the hilus (H) and until CA3c. (*c*, *d*) Scatter dot lots (mean ± SD) indicating that the number of primary dendrites (*c*) and that the dendritic angle spread (*d*) of SGC ($n = 17$, orange) is significantly larger than for GC ($n = 26$, blue; Mann and Whitney test, $P < 0.0001$). (*e*, *f*) Histograms plotting the absolute numbers of GC and SGC (*e*) and the fraction of SGC (*f*) in young adult animals ($n = 35$) as a function of the time of tamoxifen administration. The peak of SGC genesis occurs at E14,5 (*e*) earlier than that for GC which occurs around birth. Note that despite a small absolute number of SGC compared with GC (*f*), these cells represent around 40% of the fate-mapped neurons at E12.5 (*f*).

($n = 40$) and compared with randomly patched cells in the granular layer ($n = 67$). For experiments examining the firing rate, capacitance, and input resistance, cells were held at resting membrane potential, that is, the value obtained in the absence of current injection, which approximated −75 mV (Table 1). The test pulse consisted of 4 s incremented current injections from positive to negative values. We analyzed and compared the following physiological variables (see Materials and Methods): resting membrane potential (Vm), membrane resistance (Rm) and capacitance (Cm), action potential (AP) amplitude, threshold and duration, gain (i.e., the slope linking the evoked firing frequency to the injected current, *f*/*I*), the maximum firing rate, cell firing frequency adaptation, fAHP amplitude, AP firing accommodation, and rheobase. We observed a remarkable

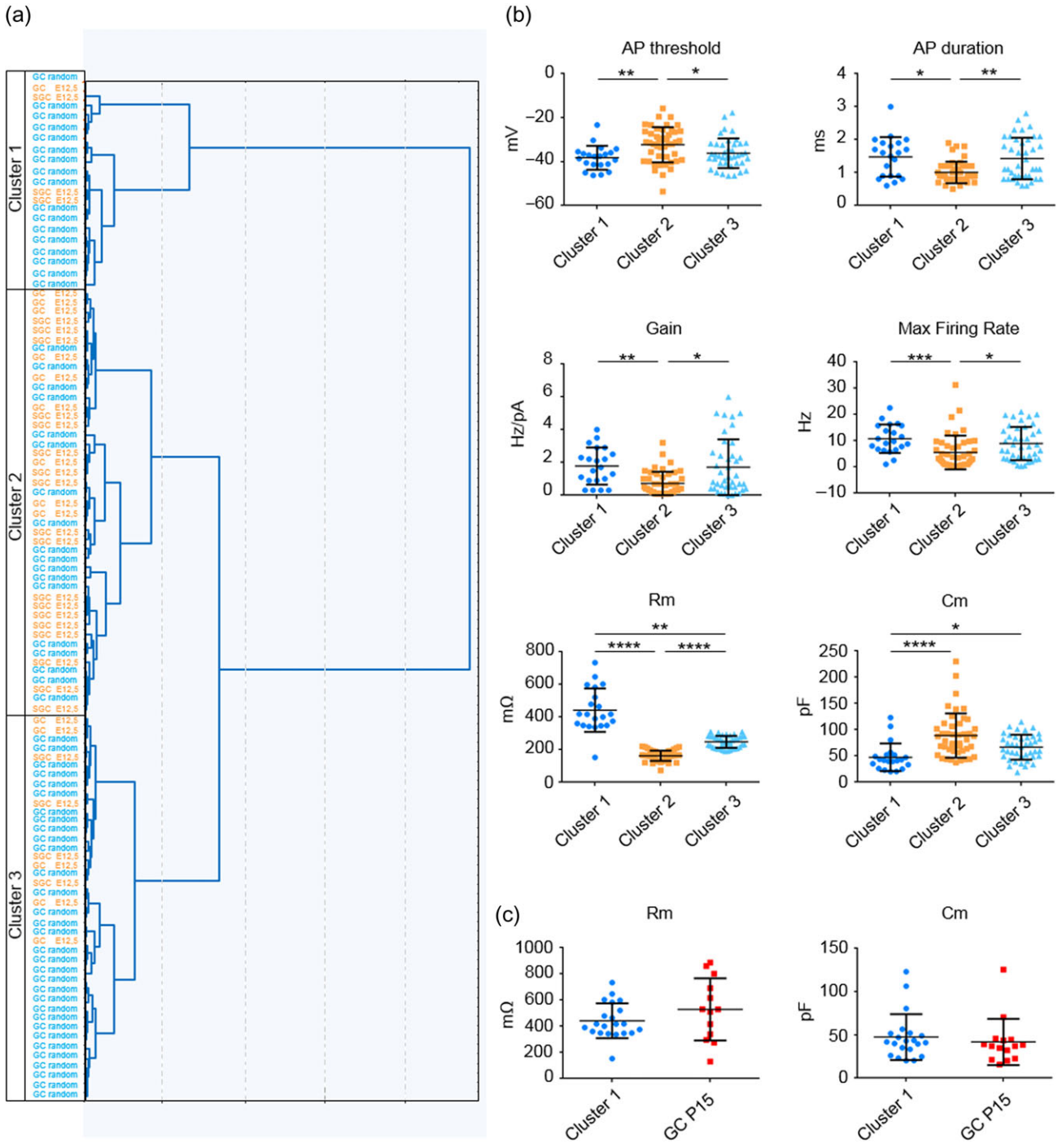

Figure 4. Cluster analysis of recorded neurons based on electrophysiological features segregates into 3 groups. (*a*) Cluster analysis tree of the electrophysiological dataset from recorded cells in the dentate gyrus ($n = 107$, Ward's method, Dlink: Euclidian distances, see Materials and Methods). Most (68%) of early born SGC and GC (orange) segregate into the same group (Cluster 2) whereas most of the random GC (blue) fall into 2 distinct clusters, clusters 1 and 3. (*b*) Scatter dot plots (mean ± SD) indicating the values of action potential (AP) threshold and duration, Gain and Maximum (Max) firing rate, membrane resistance (Rm), and capacitance (Cm) for recorded cells according to the cluster analysis. Note that cluster 2 cells display lower values of Gain, Max firing Rate, Rm and higher values for AP threshold and Cm; these physiological properties suggest that cluster 2 cells, that contain the highest number of SGC, are less excitable. Statistical analysis: Kruskal and Wallis test followed by Dunn's multiple comparisons test. (*c*) Scatter dot plots (mean ± SD) showing that the Rm and Cm values for cluster 1 cells are not different (Mann and Whitney test) from those of GC randomly recorded at P15.

heterogeneity among GC, even when sampled from temporally matched birth dates and we could not delineate any archetypic firing behavior. Cells could be classified as adapting or regular firing in both groups. However, despite such heterogeneity, ebGC significantly differed from randomly patched GC by some intrinsic electrophysiological features including a lower input resistance, a more depolarized AP threshold, a higher rheobase and a lower gain (Fig. 2 and Table 1). Altogether, these indicated

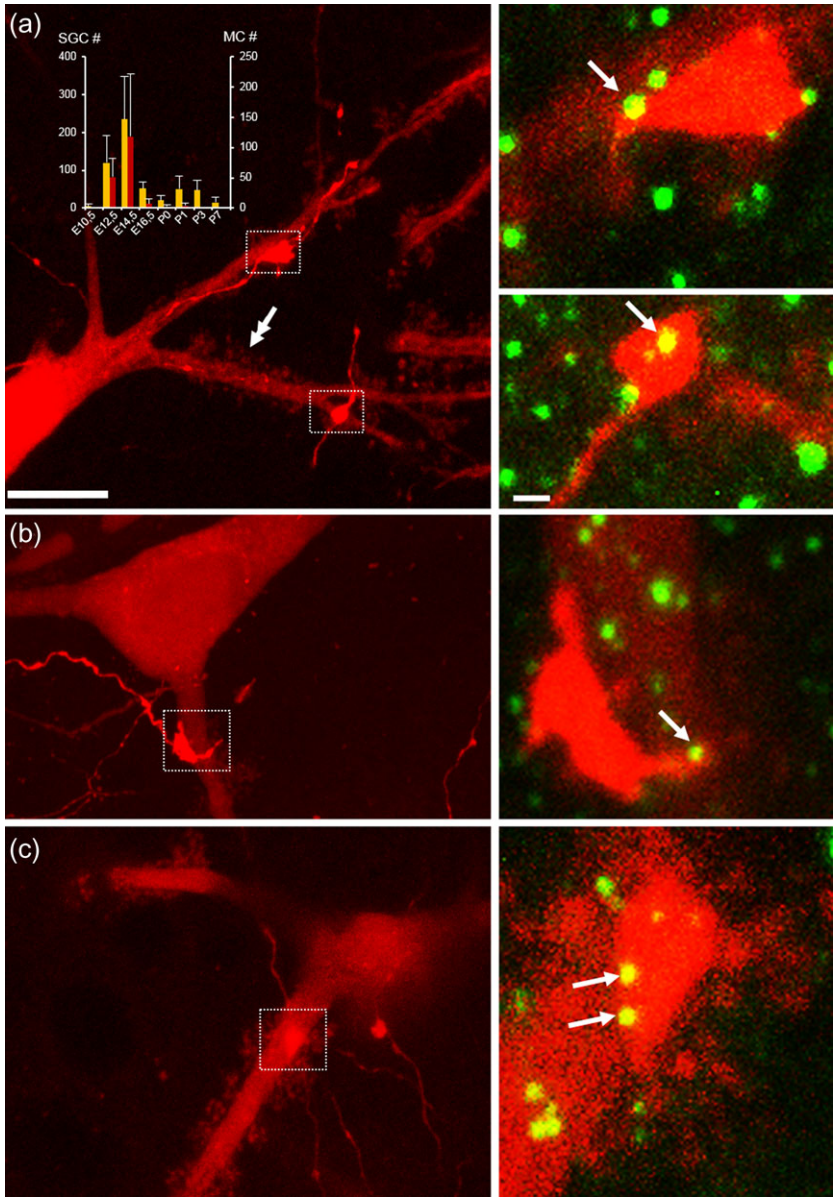

Figure 5. Early born mossy cells, SGC and GC form a temporally matched circuit in the young adult Dentate Gyrus. (*a*, *b*) Mossy cells showing typical thorny excrescences (double arrows in *a*) are labeled with Td-tomato (red) in the hilus of *Ngn2CreERTM;Ai14:LoxP* mice following tamoxifen administration at E12.5. Inset histogram in (*a*) plots the developmental profile of MC production (red) and SGC (orange) as a function of tamoxifen administration date. Numerous mossy fibers run throughout the hilus and form synaptic contacts onto mossy cell dendrites (framed areas in *a*–*c*) as suggested by PSD95 labeling (arrows, right panels). Scale bars = 10 μm (left panels) and 1 μm (right panels).

an earlier firing but lower excitability for ebGC as compared with randomly patched GC.

Early Born Cells in the DG Comprise SGC

We next asked whether ebGC could display remarkable morphological properties that would distinguish them from later-born GC. To this aim, cells were filled with Neurobiotin through the patch-pipette. A total of 53 cells were morphologically recovered post hoc and reconstructed for morphometric analysis (Table 2). We could observe 2 characteristic types of somato-dendritic morphologies. The most common type displayed a typical GC morphology with a round soma located in the granular layer and from which emerged 1 or 2 primary branches that arborized perpendicular to the granular layer (Fig. 3*a*, left and *b*). All randomly patched GC and all ebGC located in the granular layer displayed such typical morphology. The second type of labeled neuron was much less frequent and displayed the emblematic morphological features of previously described semilunar neurons (SGC; Fig. 3*a*, right and *b*; Ramon y Cajal 1909; Williams et al. 2007; Larimer and Strowbridge 2010). Their soma was located in the molecular layer and exhibited a half-moon shape. Their primary apical dendrites, more numerous than for GC, (typically from 2 to 5), emerged from the 2 extremities of the half-moon-shaped cell body and arborized throughout the molecular layer (Fig. 3*a*–*c*, Table 2). As expected (Ramon y Cajal 1909; Williams et al. 2007; Larimer and Strowbridge 2010), morphometric analysis confirmed a wider angular spacing of the

primary apical dendrites originating from SGC than from GC (170°±11° vs. 107°±6°, respectively, Fig. 3*d*). Most SGC-recovered axons ran directly through the granular layer ($n = 4$). In one case, we found an axon running horizontally in the molecular layer before reaching the granular layer but it was cut at the border with the hilus. All GC axons but one ($n = 15$), arborized in the hilus and CA3c; one ran straight towards CA3 without arborizing in the hilus. None of them were seen running or arborizing in the molecular layer. Therefore, ebGC comprise 2 morphological subtypes of cells, GC and SGC.

We next compared the developmental neurogenesis profiles of SGC and GC based on their somatic location and dendritic morphologies. In this way, we could count GC and SGC in the DG of young adult brain slices for different time points of tamoxifen gavage (see Materials and Methods; Fig. 3*e*,*f*). We observed that the number of labeled GC and SGC peaked at different time points since most GC were issued from Ngn2 progenitors labeled around birth (P0–1) while the peak was one week earlier (E14.5) for SGC (Fig. 3*e*). By pooling experiments across all age groups we could estimate that SGC represented less than 3% of all the fate-mapped glutamatergic neurons in the young adult DG (i.e., 2521 out of 104 657 cells). Nevertheless, when calculating the ratio of SGC over the entire number of neurons labeled per slice, we found that SGC represented almost half (40%) of the E12.5-labeled neurons in the DG (i.e., ebGC, Fig. 3*f*); this therefore represents a high proportion for such a rare subtype of cell. Thus, the probability for a neuronal progenitor to produce a SGC is higher at the earliest stages of DG embryogenesis. Later, more than 98% of them will produce typical GC.

Early Born Granule and Semilunar Cells Segregate Into a Distinct Physiological Subclass Despite Their Morphological Differences

To further identify functional families of DG cells without any a priori assignment of possible cell classes or of temporal origin, we next performed a cluster analysis based on all electrophysiological variables (Ward's method, Euclidian distance). Surprisingly, such analysis segregated our dataset into 3 separate groups (Table 3; Fig. 4*a*): clusters 1 and 3 mainly contained random GC (81% and 78%, respectively); in contrast, cluster 2 contained a majority of early born SGC and GC (i.e., ebGC; 60%). The mean age of the mice used in the 3 cluster groups was not significantly different and exceeded 77 postnatal days which means that neurons were recorded in young adults (Blue and Parnavelas 1983; Bähr and Wolf 1985; Sengupta 2013).

Closer inspection of the electrophysiological variables within clusters revealed that the cluster that grouped together granule cells with an early temporal origin (cluster 2) displayed a significantly higher AP threshold and faster duration together with a lower gain and maximum firing rate as compared with the other 2 clusters (Fig. 4*b*, $P < 0.005$, Kruskal–Wallis test). This indicated a lower intrinsic excitability for cells in that cluster, as expected from the fact that it mainly contained ebGC. Interestingly, the only 2 parameters that differentiated clusters 1 and 3 were the Rm and Cm, with a significantly higher Rm and lower Cm for neurons in cluster 1 (Fig. 4*b*). These 2 parameters may reflect a different stage of maturation, possibly indicating that the GC in that group could be immature cells originating from protracted postnatal neurogenesis. To test this possibility, we randomly recorded GC at juvenile stages (P15), assuming that most GC recorded in these slices would still be developing (Table 4). We observed no significant difference between Rm and Cm for GC recorded at P15 and random GC belonging to cluster 1 (Fig. 4*c*). This suggests that cluster 1 may indeed group together GC at an immature stage. Therefore, as previously shown (Schmidt-Hieber et al. 2004; Allene et al. 2012), the age of a given immature cell, determines its physiological properties, rather than the age of the recorded mouse. Still, we found a significant correlation between the age of the recorded mouse and several electrophysiological parameters indicating that DG cells continue maturing between P50 and P120 (Pearson correlation test, $P < 0,01$, Supplementary Table). This correlation was not seen among SGCs or ebGCs recorded in young adults ($P > 0,1$), suggesting that these cells were fully mature in our young adult sample age (Supplementary Table).

SGC were also targeted for patch-clamp recordings in juvenile slices (Table 4). In agreement with their early temporal origin, these cells displayed a significantly larger capacitance and smaller membrane resistance, a larger spike amplitude and a higher adaptation ratio than their GC counterparts at P15 (Table 4). In addition, in contrast to older animals, and in agreement with previous reports (Williams et al. 2007; Gupta et al. 2012), we found 2 out of 3 Neurobiotin-filled SGC at P15 with axons running horizontally in the molecular layer and exhibiting collaterals before reaching the border of the granular layer/hilus.

We conclude that early born granule cells in the DG form a distinct subpopulation of low excitability neurons uniformly scattered within the molecular and granule cell layers. In agreement with an early birthdate, these cells display more mature properties than their glutamatergic counterparts at juvenile developmental stages.

MC are Contacted by Early Born Granule Cells: Temporally Matched Circuits in the Young Adult DG

Semilunar cells were previously shown to contribute to the sustained depolarization of hilar interneurons, possibly through the activation of MC (Larimer and Strowbridge 2010). Given than MC were proposed to contribute to the earlier waves of glutamatergic neuron production in the DG (Li et al. 2008), we next asked whether they could form isochronic circuits with early born granule cells. We found that E12.5-labeled neurons in the DG comprised cells in the hilus with a typical MC morphology including the presence of thorny excrescences (Fig. 5), which do not exist on interneurons or granule cells (Scharfman 2016). We quantified the developmental profile of MC production and found that it nicely paralleled that of SGC, with a peak at E14.5 (Fig. 5*a*, inset).

We next asked whether ebGC/SGC could display functional synaptic contacts with early born MC as it has been shown that MC receive synaptic contacts from mossy terminals (Frotscher et al. 1991). To this aim, we first attempted to perform paired-recordings in E12.5 tamoxifen-treated Ngn2/Ai14 mice. However, the low number of labeled cells in the DG per slice (about 2 cells), combined to high chances to observe cut axons by the slicing made it almost impossible to get any successful recording despite several attempts ($n = 27$ mice, 12 paired-recorded cells). We therefore decided to look for putative contacts using morphological inspection of labeled cells and taking advantage of the characteristic features of mossy axons. Interestingly, close apposition of mossy terminals (Fig. 5) and/or en-passant varicosities from ebGC and/or ebSGC could frequently be observed on ebMC proximal dendrites; we found that 80% of ebMC (12 out of 15 recovered cells) received a mean of 2.5 ± 0.5 putative contacts. Using PSD95 labeling as a proxy, we observed putative synaptic contacts between mossy

terminals and MC (Fig. 5, right images). This indicates that early born granule cells and early born MC form a pioneer circuit embedded within the young adult DG.

Discussion

This study analyses the morphofunctional diversity of glutamatergic neurons in the young adult hippocampus from a developmental perspective. Using inducible genetic fate-mapping combined to unbiased multiparametric electrophysiological analysis, we uncover a functional subtype of excitatory neuron in the DG that is sparsely scattered in the granular layer and comprises critical components of the DG network, including the semilunar cells. Early born neurons in the granular layer are not intrinsically prone to be active, but together with their early born partners in the hilus, the MC, they form a hidden scaffold that may be recruited in specific conditions to gate information transfer to the hippocampus.

We find that temporal origin specifies physiology rather than morphology. Indeed, early born glutamatergic neurons issued from Ngn2-expressing embryonic progenitors were found here to develop into a morphologically diverse but electrophysiologically distinct population of granule cells. Neurons labeled after E12.5 tamoxifen administration comprised both SGC in the molecular layer and granule cells distributed throughout the granular layer. Such morphological diversity among early born cells is reminiscent of our previous observations for CA3 early born glutamatergic cells (Marissal et al. 2012) as well as for CA3 and CA1 early born GABAergic neurons (Picardo et al. 2011), which comprised cells with different dendritic and axonal arbors, different somatic locations and expressing various neurochemical contents. This finding is partly in agreement with the protomap hypothesis regarding neuronal physiology. However, it seems that morphology is not similarly specified by the time of origin. It is possible that morphological diversity is a hallmark of early born cortical neurons but not of later born cells. Here we used the temporal schedule for Ngn2 expression to label early born glutamatergic cells. It was shown that most DG neurons originate from Ngn2-expressing progenitors, a transcription factor expressed at the earliest stages of DG development (Galichet et al. 2008). It will be interesting to find out whether early born neurons are generated from a specific pool of progenitors. Increasing evidence indicates that glutamatergic neurons are issued from the same multipotent progenitors and that fate distinctions are mostly temporally controlled. Interestingly, progenitor potential was shown to be progressively, temporally restricted, with early cortical progenitors being multipotent in comparison to later ones (Lodato et al. 2015). This could partly account for the morphological diversity of early born DG neurons. However, rather than genetic predetermination, the characteristic morphological traits of SGC may well also just arise from the fact that they develop in an environment more permissive for the widening of the dendritic arbor. It could also be that, in contrast to physiology, morphological specification is specified later, for example, by the external inputs received by the cells. This would be along the lines of a "protocortex hypothesis" by which neurons are born equal and multipotent with identity imposed through external inputs and activity-dependent mechanisms (O'Leary 1989). In this perspective, SGCs morphological identity could be specified by their privileged connection to MC and dendrite targeting interneurons (see below). Early born granule cells are morphologically heterogeneous, but share a remarkable set of electrophysiological characteristics, indicating an early specification of neuronal physiology. Indeed, our unbiased multiparametric analysis segregated the granule cell population into 3 classes, one of which comprised early born granule cells with the following electrophysiological traits: 1) a higher threshold for AP generation; 2) a lower gain and lower maximal firing rate; and 3) a stronger frequency adaptation. Therefore, both active and passive intrinsic properties of these cells are different and converge into a lower probability to fire action potentials. It is interesting to note that this is in contrast with early born GABA and glutamatergic cells in CA3 which expressed a higher excitability (Picardo et al. 2011; Marissal et al. 2012). Deep CA1 pyramidal neurons, which are most likely born before their more superficial counterparts, also differed in their intrinsic membrane excitability displaying a more hyperpolarized resting membrane potential and a smaller h current (Lee et al. 2014; Maroso et al. 2016). Both characteristics, combined with a stronger inhibitory drive (Lee et al. 2014; Valero et al. 2015), may also render these cells less excitable. In the same way, granule cells originating from adult neurogenesis are less excitable as age proceeds (Alme et al. 2010). How such physiological specificity may be temporally regulated remains to be determined. Single-cells are known to display tightly orchestrated sequences of spontaneous activity patterns (Allene et al. 2012), which in turn may contribute to the maturation of physiological specificity. The other classes emerging from the clustering segregated cells that were randomly targeted, are most likely GC issued from later developmental schedules and cells that were likely to originate from adult neurogenesis. The latter assumption is supported by the fact that the passive properties of these cells, including their capacitance and resistance, were comparable to those of immature GC recorded in P15 mice. Smaller capacitances and higher resistances typically reflect more immature stages of development.

In the CA3 region of the hippocampus, early born GABAergic and glutamatergic neurons develop into specific functional subtypes that are master regulators of local networks as they include hub cells (Picardo et al. 2011) or pacemakers (Marissal et al. 2012). This finding also holds for GABAergic neurons in the developing entorhinal cortex (Mòdol et al. 2017). Here we extend this rule to the DG where early born neurons develop into semilunar cells, a cell type that was previously proposed as a cellular substrate for working memory (Larimer and Strowbridge 2010). We assert that our fate-mapped neurons comprise semilunar cells for several reasons. First, these cells recapitulate the previously described morphological traits of semilunar cells, in particular their ectopic location in the inner molecular layer and typical wider dendritic spread (Ramon y Cajal 1909; Williams et al. 2007; Gupta et al. 2012). The presence of associational axon collaterals in the inner molecular layer and granular layer (Williams et al. 2007; Gupta et al. 2012) was previously observed in a small fraction (about 30%) of biocytin-filled semilunar cells in juvenile rats (P14–25 in Williams et al. 2007, and around P30 in Gupta et al. 2012). This feature seems to be developmentally regulated since we were also able to recover such collaterals in the inner molecular layer from 66% of the cells sampled at P15, whereas the axons of cells from P60 mice and beyond could occasionally run horizontally in the molecular layer, but never displayed any collateral. Our experimental sample also displayed some of the previously reported electrophysiological characteristics of semilunar cells, including a lower resistance, but differed regarding the ratio of spike frequency adaptation (Williams et al. 2007; Gupta et al. 2012). This difference may arise from species difference, different experimental protocols, including the absence of calcium buffering in our intracellular pipette solution. Therefore, the above

observations indicate that SGC arise from the earliest stages of DG embryogenesis. Their peak of generation is around E14.5 and they represent almost half of the granule cells generated at E12.5. Interestingly, we also confirm that MC are the other archetypic subtype of DG glutamatergic neuron among the earliest generated. In addition, early born MC receive putative synaptic contacts from temporally matched granule cells and SGC. Such putative contacts can be found in 80% of the labeled MC, which is a higher ratio than the connection probability previously probed electrophysiologically (less than 10% connection probability between SGC and MC according to Williams et al. 2007). Although a comparison of connectivity across ages may better determine whether early born SGC preferentially synapse on age-matched MC, this temporally matched circuit is consistent with previous studies (Deguchi et al. 2011). In addition, we observed numerous E12.5 fate-mapped axons within the inner molecular layer, the privileged site of axonal arborization of MC (Fig. 1). Since SGC are located in the inner molecular layer, it is also possible that these cells in turn receive inputs from MC, thus, forming a close-loop circuit of pioneer neurons. In this study, the embedment of early born cells within GABAergic networks has not been examined. However, a previous study suggests that SGC may be preferentially targeted by dendrite-projecting interneurons, including somatostatin-containing ones, rather than PV-expressing perisomatic cells (Gupta et al. 2012). Given than somatostatin-expressing neurons are generated earlier than their perisomatic counterparts, with some at very early stages (Picardo et al. 2011), we can speculate that early born granule cells are also preferentially contacted by early born GABA neurons in the DG, as previously shown in CA1 for the PV innervation onto deep versus superficial pyramidal cells (Donato et al. 2015). Regardless, probably the most unique arrangement of early born granule cells, is the absence of radial layering. It is unlikely that such observation results from unspecific labeling from our method for several reasons. First, the population of granule cells labeled using this method shares common electrophysiological traits despite this layer dispersion. Second, an inside out layering pattern can still be induced with E12.5 tamoxifen injections in CA3 or in the neocortex (Fig. 1), indicating that layer dispersion is a distinctive feature in the DG. Most importantly, dispersion of the early generated granule cell cohort was previously suggested using other methods. Hence, autoradiographic labeling of the offsprings of mice exposed in utero to a pulse of tritiated thymidine (Caviness 1973), indicated that the earliest formed cells were scattered whereas later formed cells tended to be laminated (Caviness 1973), a property also observed with retrovirus labeling (Mathews et al. 2010).

Although early born granule cells are critically positioned to influence information transfer into the hippocampus, they are also less excitable. It may well be that the silent network of early born granule cells is only activated in specific conditions where context and integrated spatiotemporal information need to be bound, or alternatively in pathological conditions where their intrinsic brake is alleviated as shown for SGC in epilepsy (Gupta et al. 2012). Our study renders this unique population of cells accessible to the conditional expression of genes of interest, including optogenetic vectors or calcium indicators, which opens the way for exploring their role in vivo, in health and disease.

Authors' Contributions

L.S. and A.B. performed the experiments and analyzed the results. L.S., A.B., and R.C. designed the experiments and wrote the article. R.C. designed the project.

Supplementary Material

Supplementary material is available at *Cerebral Cortex* online.

Funding

European Research Council under the European Union's FP7 and Horizon 2020 research and innovation programs (Grant agreement nos. 242842 and 646925) as well as by the Agence Nationale pour la Recherche (ANR, Programme Blanc bilatéraux, ANR-13-ISV4-0002-01 "EbGluNet"). L.S. is funded by the "Ministere de l'Enseignement Supérieur, de la Recherche et de l'Innovation." A. B. and R.C. are supported by the Centre National de la Recherche Scientifique (CNRS).

Notes

We thank Pr. David Anderson for providing the Ngn2CreERTM mouse. We thank T. Tressard, E. Leprince, C. Pauchet, and L. Cagnacci for their technical support. We also thank S. Pellegrino-Corby, M. Kurz, T. Titus, and F. Michel from the INMED animal and imaging facilities (InMagic). *Conflict of Interest*: The authors declare no conflict of interest.

References

Allene C, Picardo MA, Becq H, Miyoshi G, Fishell G, Cossart R. 2012. Dynamic changes in interneuron morphophysiological properties mark the maturation of hippocampal network activity. J Neurosci. 32:6688–6698.

Alme CB, Buzzetti RA, Marrone DF, Leutgeb JK, Chawla MK, Schaner MJ, Bohanick JD, Khoboko T, Leutgeb S, Moser EI, et al. 2010. Hippocampal granule cells opt for early retirement. Hippocampus. 1123:1109–1123.

Altman J, Bayer SA. 1990. Migration and distribution of two populations of hippocampal granule cell precursors during the perinatal and postnatal periods. J Comp Neurol. 301: 365–381.

Angevine JB. 1965. Time of neuron origin in the hippocampal region. An autradiographic study in the mouse. Exp Neurol. (Suppl 2):1–70.

Bayer S. 1980. Development of the hippocampal region in the rat 1. Neurogenesis examined with 3h-thymidine autoradiography. J Comp Neurol. 190:87–114.

Blue ME, Parnavelas JG. 1983. The formation and maturation of synapses in the visual cortex of the rat. II. Quantitative analysis. J Neurocytol. 12:697–712.

Butt SJ, Fuccillo M, Nery S, Noctor S, Kriegstein A, Corbin JG, Fishell G. 2005. The temporal and spatial origins of cortical interneurons predict their physiological subtype. Neuron. 48:591–604.

Bähr S, Wolff JR. 1985. Postnatal development of axosomatic sy napses in the rat visual cortex: morphogenesis and quantitaive evaluation. J Comp Neurol. 233:405–420.

Caviness VS. 1973. Time of neuron origin in the hippocampus and dentate gyrus of normal and reeler mutant mice: an autoradiographic analysis. J Comp Neurol. 15:113–120.

Crespo D, Stabfiekd BB, Cowan WM. 1986. Evidence that late-generated granule cells do not simply replace earlier formed neurons in the rat dentate gyrus. Exp Brain Res. 62:541–548.

Danielson NB, Kaifosh P, Zaremba JD, Lovett-barron M, Tsai J, Denny CA, Balough EM, Goldberg AR, Drew LJ, Hen R, et al. 2016. Distinct contribution of adult-born hippocampal granule cells to context encoding. Neuron. 90:101–112.

Deguchi Y, Donato F, Galimberti I, Cabuy E, Caroni P. 2011. Temporally matched subpopulations of selectively interconnected principal neurons in the hippocampus. Nat Neurosci. 14:495–504.

Donato F, Chowdhury A, Lahr M, Caroni P. 2015. Early- and late-born parvalbumin basket cell subpopulations exhibiting distinct regulation and roles in learning. Neuron. 85: 770–786.

Donega V, Marcy G, Lo Giudice Q, Zweifel S, Angonin D, Fiorelli R, Abrous DN, Rival-Gervier S, Koehl M, Jabaudon D, et al. 2018. Transcriptional dysregulation in postnatal glutamatergic progenitors contributes to closure of the cortical neurogenic period. Cell Rep. 22:2567–2574.

Frotscher M, Seress L, Schwerdtfeger WK, Buhl E. 1991. The mossy cells of the fascia dentata: a comparative study of their fine structure and synaptic connections in rodents and primates. J Comp Neurol. 312:145–163.

Galichet C, Guillemot F, Parras CM. 2008. Neurogenin 2 has an essential role in development of the dentate gyrus. Development. 135:2031–2041.

Gupta A, Elgammal FS, Proddutur A, Shah S, Santhakumar V. 2012. Decrease in tonic inhibition contributes to increase in dentate semilunar granule cell excitability after brain injury. J Neurosci. 32:2523–2537.

Hand R, Bortone D, Mattar P, Nguyen L, Heng JI, Guerrier S, Boutt E, Peters E, Barnes AP, Parras C, et al. 2005. Phosphorylation of neurogenin2 specifies the migration properties and the dendritic morphology of pyramidal neurons in the neocortex. Neuron. 48:45–62.

Kron MM, Zhang H, Parent JM. 2010. The developmental stage of dentate granule cells dictates their contribution to seizure-induced plasticity. J Neurosci. 30:2051–2059.

Laplagne DA, Esposito MS, Piatti VC, Morgenstern NA, Zhao C, Van Praag H, Gage FH, Schinder AF. 2006. Functional convergence of neurons generated in the developing and adult hippocampus. PLoS One. 4:e409.

Laplagne DA, Kamienkowski JE, Espósito MS, Piatti VC, Zhao C, Gage FH, Schinder AF. 2007. Similar GABAergic inputs in dentate granule cells born during embryonic and adult neurogenesis. Eur J Neurosci. 25:2973–2981.

Larimer P, Strowbridge BW. 2010. Representing information in neuronal cell assemblies: persistent activity in the dentate gyrus mediated by semilunar granule cells. Nat Neurosci. 13:213–222.

Lee SH, Marchionni I, Bezaire M, Varga C, Danielson N, Lovett-Barron M, Losonczy A, Soltesz I. 2014. Parvalbumin-positive basket cells differentiate among hippocampal pyramidal cells. Neuron. 82:1129–1144.

Li G, Berger O, Mercedes SH, Wu PN, Pleasure SJ. 2008. Hilar mossy cells share developmental influences with dentate granule neurons. Dev Neurosci. 30:255–261.

Lodato S, Shetty AS, Arlotta P. 2015. Cerebral cortex assembly: generating and reprogramming projection neuron diversity. Trends Neurosci. 38:117–125.

Madisen L, Zwingman TA, Sunkin SM, Oh SW, Hatim A, Gu H, Ng LL, Palmiter RD, Hawrylycz MJ, Allan R, et al. 2010. A robust and high-throughput Cre reporting and characterization system for the whole mouse brain. Nat Neurosci. 13: 133–140.

Marissal T, Bonifazi P, Picardo MA, Nardou R, Petit LF, Baude A, Fishell GJ, Ben-Ari Y, Cossart R. 2012. Pioneer glutamatergic cells develop into a morpho-functionally distinct population in the juvenile CA3 hippocampus. Nat Commun. 3:1316.

Maroso M, Szabo GG, Kim HK, Alexander A, Bui AD, Lee S, Lutz B, Soltesz I. 2016. Cannabinoid control of learning and memory through hcn channels. Neuron. 89:1059–1073.

Mathews EA, Morgenstern NA, Piatti VC, Zhao C, Jessberger S, Schinder AF, Gage FH. 2010. A distinctive layering pattern of mouse dentate granule cells is generated by developmental and adult neurogenesis. J Comp Neurol. 518: 4479–4490.

Miyoshi G, Hjerling-leffler J, Karayannis T, Sousa VH, Butt JB, Battiste J, Johnson JE, Machold RP, Fishell G. 2010. Genetic fate mapping reveals that the caudal ganglionic eminence produces a large and diverse population of superficial cortical interneurons. J Neurosci. 30:1582–1594.

Mòdol L, Sousa VH, Malvache A, Tressard T, Baude A, Cossart R. 2017. Spatial embryonic origin delineates gabaergic hub neurons driving network dynamics in the developing entorhinal cortex. Cereb Cortex. 27:4649–4661.

Nakashiba T, Cushman JD, Pelkey KA, Renaudineau S, Buhl DL, Mchugh TJ, Barrera VR, Chittajallu R, Iwamoto KS, Mcbain CJ, et al. 2012. Young dentate granule cells mediate pattern separation whereas old granule cells contribute to pattern completion. Cell. 149:188–201.

Nord AS, Pattabiraman K, Visel A, Rubenstein JL. 2015. Genomic perspectives of transcriptional regulation in forebrain development. Neuron. 85:27–47.

Ozen I, Galichet C, Watts C, Parras C, Guillemot F, Raineteau O. 2007. Proliferating neuronal progenitors in the postnatal hippocampus transiently express the proneural gene Ngn2. Eur J Neurosci. 25:2591–2603.

O'Leary DDM. 1989. Do cortical areas emerge from a protocortex? Trends Neurosci. 12:400–406.

Picardo MA, Guigue P, Bonifazi P, Batista-Brito R, Allene C, Ribas A, Fishell G, Baude A, Cossart R. 2011. Pioneer GABA cells comprise a subpopulation of hub neurons in the developing hippocampus. Neuron. 71:695–709.

Rakic P. 1972. Mode of cell migration to the superficial layers of fetal monkey neocortex. J Comp Neurol. 145:61–84.

Rakic P. 1988. Specification of cerebral cortical areas. Science. 241:170–176.

Rakic P, Ayoub AE, Breunig JJ, Dominguez MH. 2009. Decision by division: making cortical maps. Trends Neurosci. 32: 291–301.

Rakic P, Nowakowski RS. 1981. The time of origin of neurons in the hippocampal region of the rhesus monkey. J Comp Neurol. 196:99–128.

Ramon y Cajal S. 1909. Histologie du système nerveux de l'homme et des vertébrés. Paris: Maloine.

Scharfman HE. 2016. The enigmatic mossy cell of the dentate gyrus. Nat Rev Neurosci. 17:562–575.

Schlessinger AR, Cowan WM, Gottlieb DI. 1975. An autoradiographic study of the time of origin and the pattern of granule cell migration in the dentate gyrus of the rat. J Comp Neurol. 156:149–175.

Schmidt-Hieber C, Jonas P, Bischofberger J. 2004. Enhanced synaptic plasticity in newly generated granule cells of the adult hippocampus. Nature. 429:184–187.

Sengupta P. 2013. The laboratory rat: relating its age with human's. Int J Prev Med. 4:624–630.

Valero M, Cid E, Averkin RG, Aguilar J, Sanchez-aguilera A, Viney TJ, Gomez-dominguez D, Bellistri E, Menendez de la Prida L. 2015. Determinants of different deep and superficial CA1 pyramidal cell dynamics during sharp-wave ripples. Nat Neurosci. 18:1281–1290.

Villette V, Guigue P, Picardo MA, Sousa VH, Leprince E, Lachamp P, Malvache A, Tressard T, Cossart R, Baude A. 2016. Development of early-born γ-Aminobutyric acid hub neurons in mouse hippocampus from embryogenesis to adulthood. J Comp Neurol. 524:2440–2461.

Williams PA, Larimer P, Gao Y, Strowbridge BW. 2007. Semilunar granule cells: glutamatergic neurons in the rat dentate gyrus with axon collaterals in the inner molecular layer. J Neurosci. 27:13756–13761.

Zirlinger M, Lo L, McMahon J, McMahon AP, Anderson DJ. 2002. Transient expression of the bHLH factor neurogenin-2 marks a subpopulation of neural crest cells biased for a sensory but not a neuronal fate. Proc Nat Acad Sci USA. 99: 8084–8089.